Optic Nerve Head Morphology and Macula Ganglion Cell Inner Plexiform Layer Thickness in Axially Anisometropic Rhesus Monkeys

Zhihui She, Krista M. Beach, Li-Fang Hung, Lisa A. Ostrin, Earl L. Smith III, and Nimesh B. Patel

University of Houston College of Optometry, Houston, Texas, United States

Correspondence: Nimesh B. Patel, University of Houston College of Optometry, 4401 Martin Luther King Blvd., Houston, TX 77204, USA; npatel@central.uh.edu.

Received: April 3, 2024
Accepted: August 9, 2024
Published: August 29, 2024

Citation: She Z, Beach KM, Hung LF, Ostrin LA, Smith EL III, Patel NB. Optic nerve head morphology and macula ganglion cell inner plexiform layer thickness in axially anisometropic rhesus monkeys. *Invest Ophthalmol Vis Sci.* 2024;65(10):44. https://doi.org/10.1167/iovs.65.10.44

Purpose. The purpose of this study was to determine the effects of axial elongation on optic nerve head morphology and macula inner retinal thickness in young rhesus monkeys.

Methods. Both eyes of 26 anisometropic, 1-year-old rhesus monkeys were imaged using optical coherence tomography (OCT). Before imaging, the animals were sedated, their eyes were dilated, and axial length was measured using an optical biometer. OCT imaging included a 20 degrees, 24-line radial scan centered on the optic nerve head (ONH) and two 20 degrees × 20 degrees raster scans, one centered on the ONH and the other on the macula. Radial scans were analyzed using programs written in MATLAB to quantify the Bruch's membrane opening (BMO) area and position, minimum rim width (MRW), anterior lamina cribrosa surface (ALCS) position, size of any scleral crescent, circumpapillary retinal nerve fiber layer (RNFL), and choroid thickness (pCh). Macula total retinal thickness (mTRT) and ganglion cell inner plexiform layer (GCIPL) thicknesses were quantified from macula scans. Linear least square regression was determined for OCT measures and axial length of the right eye, and for inter-eye differences.

Results. Animals were 341 ± 18 days old at the time of imaging. BMO area ($R^2 = 0.38$), ALCS position ($R^2 = 0.45$), scleral crescent area ($R^2 = 0.35$), pCh thickness ($R^2 = 0.21$), mTRT ($R^2 = 0.24$), and GCIPL thickness ($R^2 = 0.16$) were correlated with the axial length (all $P < 0.05$). For each of these parameters, the right-eye regression slope did not differ from the slope of the interocular difference ($P > 0.57$).

Conclusions. There are posterior segment morphological differences in anisometropic rhesus monkeys related to axial length. Whether these differences increase the risk of pathology remains to be investigated.

Keywords: axial elongation, nonhuman primates, ocular morphology, optic nerve head (ONH), macula

Myopia, or nearsightedness, occurs when the optics of the anterior segment focus light from a distant object in front of the retina when accommodation is relaxed. Axial elongation is the main contributing factor, and it is estimated that the worldwide prevalence of myopia will reach 50% by 2050.[1] Although refractive visual impairment can be managed with spectacles, contact lenses, or refractive surgery, these options do not address the anatomic changes associated with axial elongation and the related risks for ocular complications.[2]

Clinical studies show that axial elongation is negatively correlated with macula/parafoveal thickness and volume,[3–8] choroidal thickness,[9–12] and macular vascular density.[13,14] In addition to the macula region, the optic nerve head (ONH) morphology is also altered in longer eyes. Myopic eyes often have an increased optic disc size,[15,16] tilting of the nerve,[17] a more anterior lamina cribrosa surface,[18] and temporal crescents.[19] These structural alterations are hypothesized to increase the eye's susceptibility to ocular pathology, including mechanical stress from intraocular pressure and ganglion cell damage.

Population-based studies have identified myopia as a significant and independent risk factor for open-angle glaucoma.[20–26] Whereas glaucoma risk is thought to increase by approximately 20% with each diopter, the relationship is nonlinear, significantly increasing past 6 diopters of myopia.[27] Both myopia and glaucoma have posterior segment and peripapillary connective tissue alterations,[28] but the pathophysiology linking the two remains unknown.

Animal models of emmetropization could provide methods for determining the link between the two conditions. Although there are some notable differences, the rhesus monkey (*Macaca mulatta*) has similar ocular structure and biomechanical response to that of humans.[29] Whereas several studies have examined ocular growth and development, there is a lack of data on axial elongation and posterior segment structure in this animal model.[30,31] We hypothesize that axial elongation in this animal model has similar

posterior segment morphological features to that commonly reported in human clinical studies. Using optical coherence tomography (OCT), we present the relationship between posterior eye morphology and axial length in a group of young rhesus monkeys with visually induced experimental anisometropia.

Materials and Methods

Subjects

Subjects included 26 rhesus monkeys (*Macaca mulatta*), previously used in experiments of refractive error from 3 weeks to 6 months of age.[32–34] In these prior experiments, the majority of animals were reared wearing vision-altering goggles to induce myopic refractive errors in their right eyes.[32–34] Following this experimental period, visual interventions were removed, and the animals were reared in a standard colony environment, as previously described.[35] At the time of imaging and image processing, the imaging team (authors N.P. and Z.S.) was blinded to the prior visual experience of the animal. For this cross-sectional study, animals were imaged at a single timepoint, 6 months after removal of the vision-altering goggles (mean age of 347 ± 18 days). At this time point, the majority of anisometropic recovery is complete and the rate of axial elongation has slowed, and is similar between the two eyes.[32,36] Further, this time point was selected as maturational changes in retinal thickness have stabilized. All animal care procedures were reviewed and approved by the Institutional Animal Care and Use Committee of the University of Houston and adhered to the ARVO Statement for the Use of Animals in Ophthalmic and Vision Research.

Animal Preparation

Animals were fasted for at least 12 hours before sedation, and free access to water was allowed during this time. An intramuscular injection of ketamine (20–25 mg/kg) and xylazine (0.2–0.4 mg/kg) was administered while the animals were gently restrained in their home cages. After transporting them to the imaging laboratory, they were placed on an imaging table over a waterbed heater, and a subcutaneous injection of atropine sulfate (0.04 mg/kg) was administered to minimize salivation and maintain their heart rate. At this systemic dose, atropine does not cause pupil dilation. Instead, pupils were dilated with 1% tropicamide, and an eyelid speculum was used to keep the eyes open. Heart rate, blood pressure, and oxygen saturation were monitored continuously for the duration of the experiment. At the end of the imaging session, the effect of xylazine was reversed with atipamezole (0.03 mg/kg). The animals were then recovered in a temperature-controlled incubator before returning to their home cages.

Ocular Biometry

An optical interferometric biometer (LenStar LS900; Haag-Streit, Koeniz, Switzerland) was used to measure corneal curvature, anterior chamber depth, lens thickness, and axial length. These measures were obtained at a separate session, nominally ±3 weeks from the time of OCT imaging. Six well-centered scans were acquired for each eye and averaged. In addition to axial length correlations, biometry measures were used to calculate individual transverse retinal scaling for OCT imaging. In brief, for each eye, a three-surface schematic eye was constructed using the biometric data, and transverse scaling was calculated (in µm/deg) using the distance of the second nodal plane to the retina.[37]

Optical Coherence Tomography Imaging

Prior to imaging, a custom plano-powered, gas permeable contact lens was placed on the cornea to maintain optical clarity. OCT images were acquired using the small eye and high-resolution settings (Spectralis; Heidelberg Engineering, Heidelberg, Germany, central wavelength = 870 nm, 51.2 A-scans/deg). Scans acquired included a 24-line 20 degrees × 20 degrees radial scan and a 193-line 20 degrees × 20 degrees raster scan centered on the ONH, and a 193-line 20 degrees × 20 degrees raster scan centered on the macula. Radial scans were acquired with b-scan averaging of 20 frames, and 9 frame averaging was used for both raster scans. Only scans with signal quality above 30 decibels (dB) were used for analysis.

Image Analysis

Scans were exported as ".vol" files and analyzed using programs written in MATLAB. To minimize bias, b-scans were segmented using neural networks trained on a DeepLabv3+ network based on ResNet-50, details of which have been previously published.[38–41] The output segmentation for only the Bruch's membrane opening (BMO) was inspected for errors, and corrected as needed. Corrections were made by a trained observer (author N.P.), who was masked from the individual animal's prior visual treatment at the time of image analysis. Prior to morphological analysis, individualized transverse scaling using a three-surface schematic eye was incorporated.

Each of the radial b-scans (Fig. 1A) was compensated for light attenuation (Fig. 1B) prior to processing with the neural networks (Fig. 1C).[38,42] The BMO area was computed from the best-fit ellipse to all identified BMO locations. For each radial b-scan, the minimum rim width (MRW) was calculated as the average of all perpendicular distances from the BMO to the inner limiting membrane (ILM). To accurately represent the neural rim tissue, the MRW was confined to locations inside the BMO. The BMO position was determined as the perpendicular distance of the BMO to a 4 mm reference line aligned to the Bruch's membrane (BM) and centered on the BMO. Using the BMO as a reference, the anterior lamina cribrosa surface (ALCS) position was determined for the central 50% of the 2 BMO points. Although the posterior border of the lamina was visible in many sections (see Figs. 1B, 1C), its thickness was not quantified due to variability in visibility. Peripapillary choroid thickness (pCh) was determined for a 500 to 1000 µm annulus from the BMO. For each two-dimensional analysis, data from each b-scan were weighted equally toward determining the average thickness and position metrics.

Raster scans centered on the ONH were segmented using a neural network that labeled the ILM, nerve fiber layer (NFL), and BM.[39] The outer edges of the area devoid of BM was marked as the BMO. The circumpapillary retinal nerve fiber layer (RNFL) thickness was extracted from an interpolated scan path 550 µm from the BMO, as previously described (Fig. 2A).[43] Using the BM segmentation as a reference, a 100-micron enface slab was extracted from the OCT data to visualize any scleral crescent. When present, scleral

Investigative Ophthalmology & Visual Science

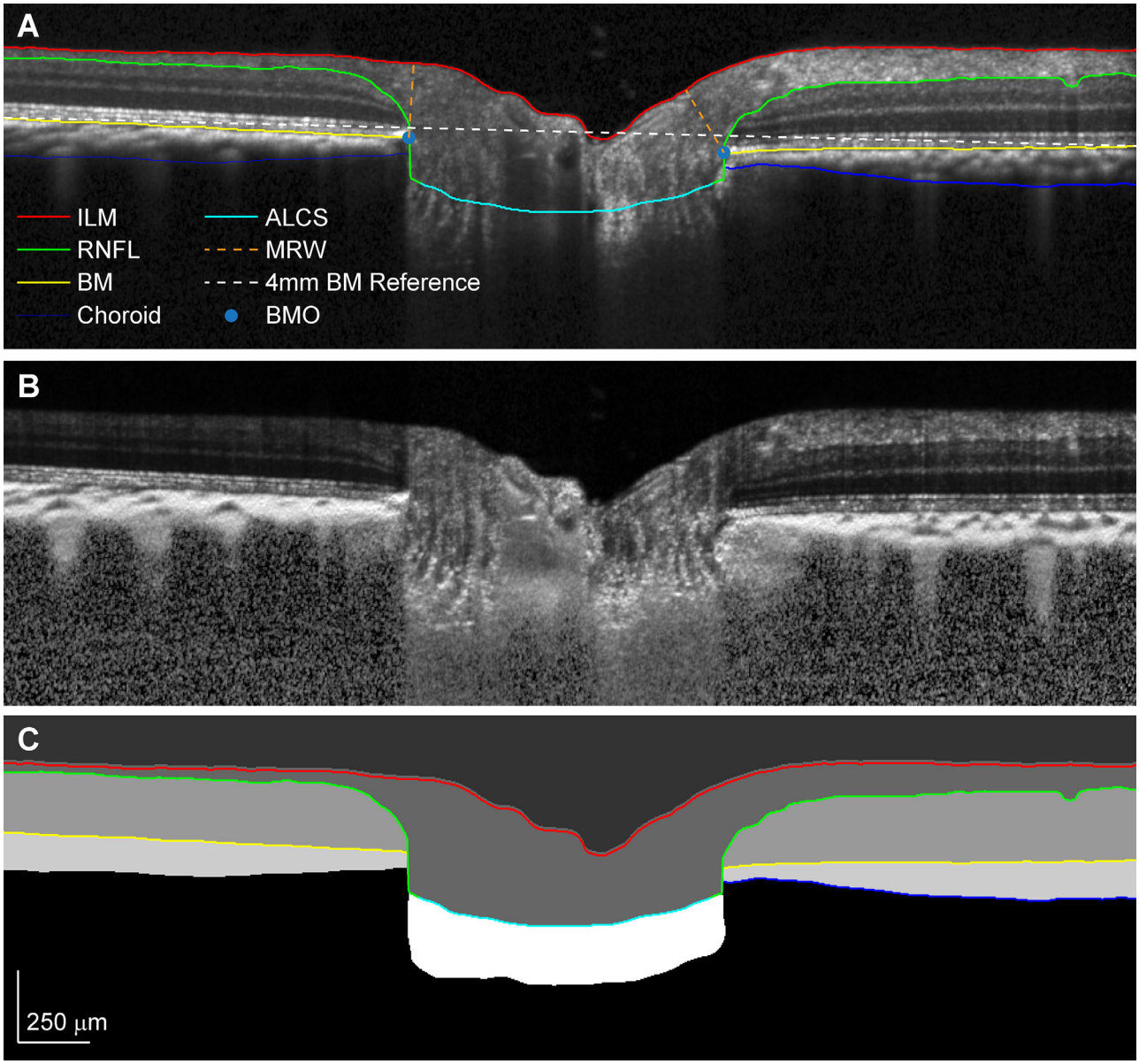

Figure 1. (**A**) OCT radial section through the center of the optic nerve with segmentation for the ILM, RNFL, and BM. The *orange dashed line* illustrates the minimum rim width, and the *white dashed line* is the 4 mm reference plane used to quantify BMO position. (**B**) B-scans were compensated for light attenuation, prior to semantic segmentation using a neural network (**C**).

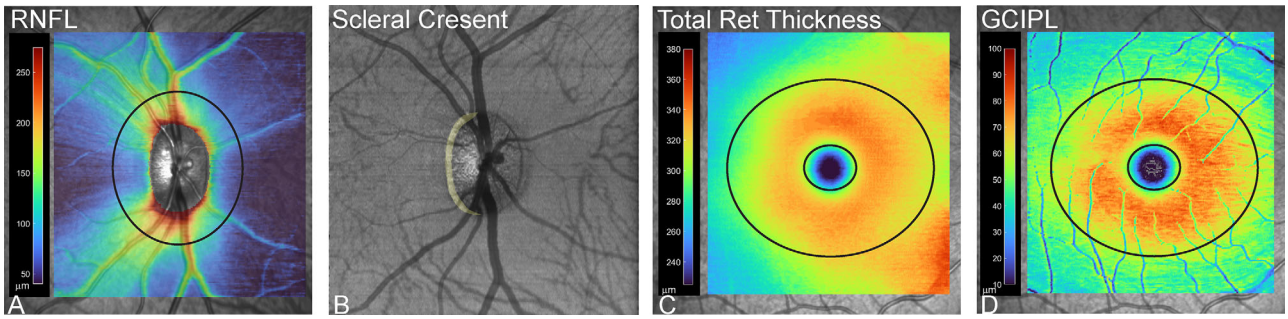

Figure 2. (**A**) RNFL thickness map illustrating the 550 µm elliptical scan path used to quantify circumpapillary RNFL thickness. (**B**) Scleral crescent, indicated in *yellow*, manually marked on an OCT slab projection from the same OCT volume as **A**. (**C, D**) Macula total retinal and GCIPL thickness, with inner and outer elliptical bounds used for quantification.

Investigative Ophthalmology & Visual Science

crescents were manually delineated, and the area was quantified (Fig. 2B).

Macula scans were segmented to identify the BM, ILM, NFL, and inner plexiform layer border. The center of the fovea was manually marked, and an elliptical annulus with an inner limit of radii 375 and 450 µm, and outer limit of 1500 and 1800 µm were used to determine the average macula total retinal thickness (mTRT) and ganglion cell inner plexiform layer (GCIPL) thickness (see Figs. 2C, 2D). The annular region was selected to match that used for human analysis of GCIPL thickness, scaled for nonhuman primate eyes, which are approximately 0.75 the size of human eyes.[44] The major retinal vasculature was included with the NFL segmentation for consistency with optic nerve scans. Hence, GCIPL thickness maps appear with focal thinning in the regions with retinal vasculature (see Fig. 2D).

Data Analysis and Statistics

Only global metrics are used for OCT measures to minimize false positive results from multiple comparisons. Least-square linear regression was used to determine the association between right eye axial length and OCT quantified measures. The initial analysis only included data from the right eye, which are suitable for studying structure-axial length correlation because their axial length spread over a larger range than the left eyes. In addition to right eye data, the interocular difference data (OCT structure and axial length) were also assessed for statistically significant regressions ($P < 0.05$). Because the two eyes of an animal are genetically identical and the developments of their refractive error are relatively independent, analysis of the interocular difference should corroborate right-eye data by reducing the influence of intersubject variability. Unless otherwise stated, the mean ± standard deviation are presented, along with 95% confidence intervals for regression data. All statistics were performed using GraphPad Prism 9.5 (GraphPad Software, LLC). The supplementary Excel file has data on each animal's OCT and axial length.

Results

Axial Length

The right eyes (mean ± standard deviation = 17.87 ± 0.99 mm) were, on average, longer than the left (17.59 ± 0.90 mm, paired *t*-test, $P = 0.02$), with the right eye minus the left eye difference in axial length ranging from −1.7 mm to 0.62 mm. Of the 26 animals, 14 had greater axial lengths in the right eyes compared to the left eyes (>0.04 mm between eye difference), 7 animals had greater axial lengths in the left eyes, whereas the rest of the animals had less than 0.04 mm between eye difference. The interocular differences in axial length were consistent, with the majority of animals having been previously reared with a right-eye myopic stimulus.

Right Eye OCT Metrics and Axial Length

Table 1 summarizes the linear regressions for each OCT metric and axial length for the right eyes. The data show that longer eyes have larger scleral crescents ($R^2 = 0.35$, $P < 0.05$), a larger BMO area ($R^2 = 0.38$, $P < 0.05$), with a more anteriorly displaced lamina ($R^2 = 0.45$, $P < 0.05$), and thinner peripapillary choroid ($R^2 = 0.21$, $P < 0.05$). Although the position of the lamina referenced to the BMO was related to axial length, the relative position of the BMO was not correlated with axial length ($P = 0.91$). Further, the correlation of axial length with MRW and RNFL thickness was not statistically significant ($P > 0.05$). However, the macula total retinal and GCIPL thicknesses were negatively correlated with axial length ($P < 0.05$).

Interocular Differences

OCT metrics from the right and left eyes in normal control animals are expected to be highly correlated. Hence, interocular differences (right eye data minus left eye data) of axial length and OCT metrics in the experimental animals should reflect the influence of axial elongation on ONH and retinal morphology. Further, the axial length versus OCT morphology slopes observed for the right eyes should be similar for interocular differences if the transverse scaling methods are accurate. Only statistically significant OCT metrics from Table 1 were assessed for this analysis. One animal did not have radial scans for the left eye, so the analysis was limited to the 25 animals with complete datasets. The correlation of inter-eye differences in axial length and OCT metrics was statistically significant for each measure, other than for the peripapillary choroid thickness ($P = 0.50$). Further, the right-eye and inter-eye correlation slopes were not statistically different for any of the metrics ($P > 0.57$). Table 2 summarizes these inter-eye correlations, and Figures 3 and 4 (ONH and macula data, respectively) illustrate the right eye and inter-eye differences for the statistically significant relationships in Table 1.

Table 1. Linear Regression of Axial Length and OCT Metrics

OCT Measure	Slope (95% CI)	Intercept (95% CI)	R^2	*P* Value
BMO area, mm^2	0.14 (0.06 to 0.22)	−1.28 (−2.56 to 0.07)	0.38	<0.01*
BMO position, µm	0.9 (−14.5 to 16.3)	42.1 (−2.7 to 0.07)	<0.01	0.91
ALCS position, µm	−41 (−60.2 to −21.8)	977.3 (633.2 to 1321)	0.45	<0.01*
Crescent, mm^2	0.09 (0.04 to 0.14)	−1.39 (−2.30 to −0.47)	0.35	<0.01*
pCh thickness, µm	−4.1 (−7.5 to −0.8)	150.7 (90.7 to 210.7)	0.21	0.02*
MRW, µm	0.9 (−12.2 to 13.9)	286 (52.8 to 519.5)	<0.01	0.89
RNFL, µm	−0.4 (−3.9 to 3.1)	126.3 (63.4 to 189.1)	<0.01	0.80
mTRT, µm	−5.5 (−9.6 to −1.4)	425.3 (351.7 to 499)	0.24	0.01*
GCIPL, µm	−1.4 (−2.8 to 0)	95.3 (70.2 to 120.3)	0.16	0.04*

ALCS, anterior lamina cribrosa surface; BMO, Bruch's membrane opening; GCIPL, ganglion cell inner plexiform layer; MRW, minimum rim width; mTRT, macula total retinal thickness; pCh, peripapillary choroid; RNFL, retinal nerve fiber layer.
* Slopes that were statistically significant.

Investigative Ophthalmology & Visual Science

Table 2. Linear Regression of Inter-Eye Differences of Axial Length and OCT Metrics

OCT Measure	Slope (95% CI)	Intercept (95% CI)	R^2	*P* Value
BMO area, mm^2	0.16 (0.11 to 0.20)	−0.03 (−0.06 to 0.0)	0.70	<0.01*
ALCS position, µm	−31.6 (−46.4 to −16.7)	−1.7 (−11.1 to 7.7)	0.46	<0.01*
Crescent, mm^2	0.09 (0.01 to 0.16)	0.03 (−0.02 to 0.08)	0.21	0.02*
pCh thickness, µm	1.1 (−2.2 to 4.4)	−0.3 (−2.4 to 1.7)	0.02	0.50
mTRT, µm	−5.4 (−8.9 to −1.9)	−0.4 (−2.6 to 1.8)	0.31	<0.01*
GCIPL, µm	−1.6 (−2.6 to −0.7)	−0.1 (−0.7 to 0.3)	0.35	<0.01*

ALCS, anterior lamina cribrosa surface; BMO, Bruch's membrane opening; GCIPL, ganglion cell inner plexiform layer; mTRT, macula total retinal thickness; pCh, peripapillary choroid.
* Slopes that were statistically significant.

Discussion

In primates, the retinal neurons and ocular morphology continue to mature early in life.[45–49] During this period of development and emmetropization, there is scleral shell expansion, with associated changes in ONH and retinal layer structure.[37,50,51] Myopia is a refractive condition that occurs when the scleral shell expands beyond the refractive power of the anterior segment and is linked to many ocular pathologies, including glaucoma.[20–27] However, the pathophysiology of this association remains elusive. Animal models may aid in determining features of the ONH and macula inner retinal thickness, which places some eyes at a higher risk of glaucoma. In this experiment, using year old animals with anisometropic axial elongation, we show that longer eyes have a larger BMO with greater scleral crescent areas, and a more anteriorly positioned lamina surface. Although measures of the peripapillary nerve fiber layer and MRW were not related to axial length, longer eyes had thinner macula inner retinal thickness.

OCT morphometrics are typically analyzed for one eye, as measures from the genetically identical fellow eye are highly correlated.[52] Several population studies in children showing inter-ocular differences in OCT metrics, are often not adequately corrected for ocular magnification.[53,54] Hence, to evaluate axial length-specific associations, in addition to single eye analysis, we analyzed the interocular difference for significant relationships using ocular magnification corrected measures. Such interocular differences are commonly analyzed in refractive error studies to better identify the effects of monocular treatments, with the assumption that eye developments in monocularly treated animals are independent of each other. When applied to morphological data, the interocular difference metric reduces the influence of individual variability in structural dimensions and biological development. Hence, the interocular difference agreeing with the single, right eye, analysis further supports the idea that scleral expansion alters posterior structure as measured by OCT.

Human, in vivo OCT and cadaveric studies show that during infancy, along with globe expansion, there is an increase in the size of the ONH.[16,51,55] The increase in ONH size is linear in eyes with low to moderate myopia, but becomes nonlinear in individuals with high myopia.[15,56] The monkeys in the current study did not have signs of pathological myopia, and, hence, only the linear component was realized for the relationship between BMO area and axial length (see Figs. 3A, 3B). Although the size of the BMO reflects on the underlying scleral opening,[57] due to variability in visualization of the scleral canal, we were unable to accurately quantify the scleral opening diameter for the current study. Addition of this metric would have enabled quantification of the relative positions of the ONH openings, whose offset increases with axial length.[58–60] A morphological feature related to opening-offset development is scleral crescent,[61] for which the distance from the temporal edge of the crescent to the fovea is not related to axial length, but the distance from the edge of the nerve to the fovea is.[19] In the primate model, based on manual delineation on an OCT enface slab, the scleral crescent was linearly related to axial length (see Figs. 3E, 3F). However, the development of a scleral crescent in young rhesus monkeys is heterogenous, with some animals not developing this feature, but having large interocular differences in axial length (see Supplementary Data).

Although the size of the ONH has been hypothesized to be a risk factor for glaucoma development, this has not been substantiated, even in anisometropic eyes.[62–65] However, in addition to ONH enlargement, axial elongation is associated with thinning of the posterior pole sclera, peripapillary scleral flange, and lamina cribrosa.[66–68] As the scleral canal enlarges with axial elongation, the lamina is thought to become taught, and is anteriorly displaced. This is supported by human studies showing that hyperopic eyes have a more posterior lamina than myopia.[18] Similarly, the right eye and interocular difference data show that the lamina of longer eyes have a more anterior ALCS position when referenced to the BMO. However, the position of the BMO referenced to the BM plane was not correlated with axial length. This suggests that the anterior displacement of the lamina is likely a reflection of radial rather than lateral strain. In fact, the relationship between BMO area and ALCS position had a negative slope and was statistically significant ($R^2 = 0.22$, $P = 0.01$, data not shown).

Although several features of the ONH were related to axial length, the MRW and peripapillary RNFL thickness were not, which is comparable to previous work in this animal model.[43] Specifically, whereas the RNFL thickness from standard circular 12 degree diameter scans is shown to be negatively correlated with axial length, this was not the case when lateral scaling was included, and scan paths extrapolated from a fixed distance from the BMO.[43] These findings are similar to human studies, which show that the relationship between circumpapillary RNFL thickness scans from 12 degree diameter circular scans and axial length can be explained by ocular magnification.[69–71] As circumpapillary RNFL thickness and MRW correlate with total retinal ganglion cell axon count in the optic nerve,[72] the data suggest that axial elongation in these subjects did not result in retinal ganglion cell loss. Hence, the results of the current

Investigative Ophthalmology & Visual Science

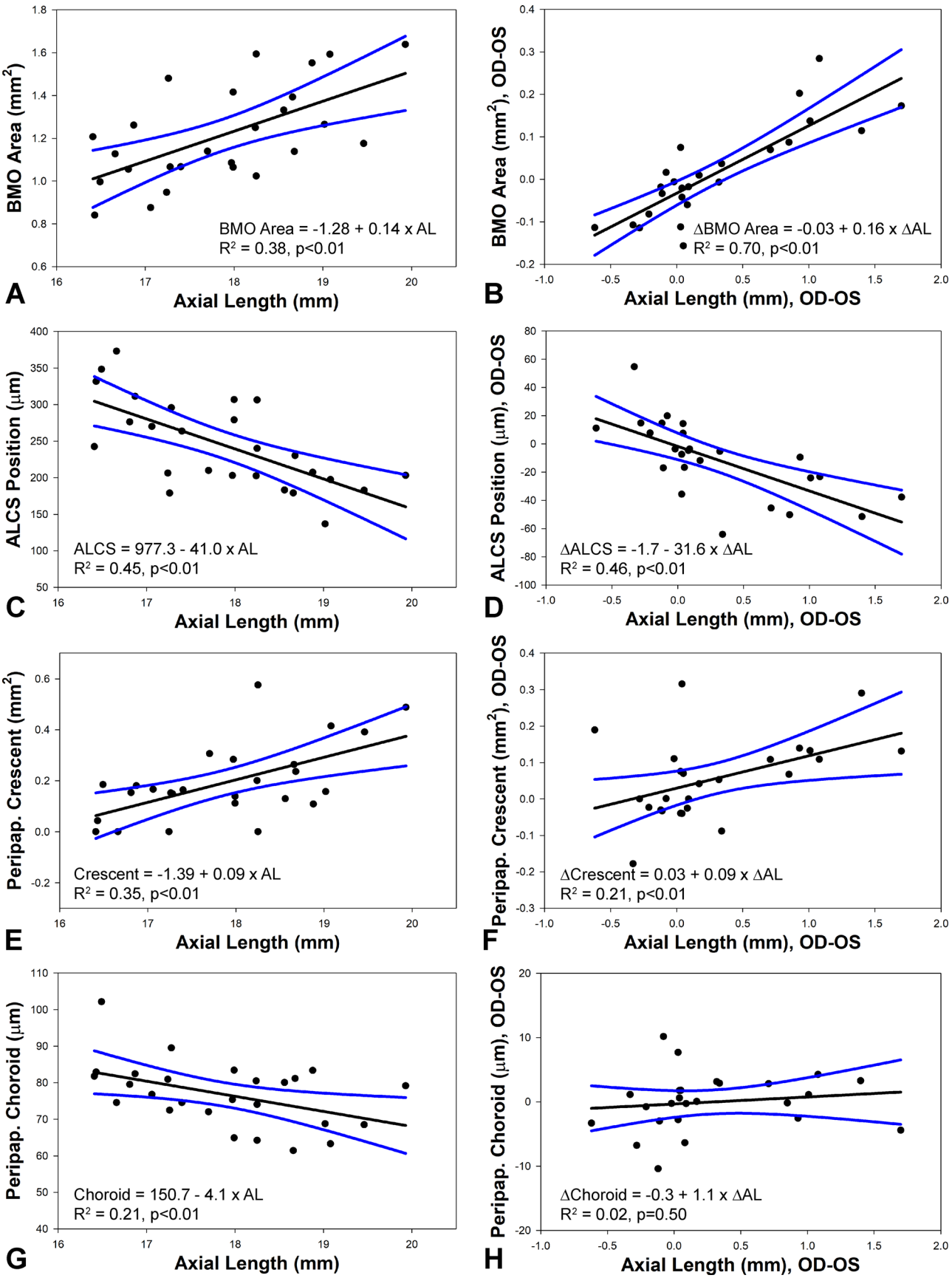

Figure 3. Right eye and interocular difference correlations with axial length and BMO area (**A, B**), ALCS position (**C, D**), Peripapillary scleral crescent (**E, F**), and pCh thickness (**G, H**). *Blue lines* illustrate the 95% confidence interval for the slope of the function. ALCS, anterior lamina cribrosa surface; BMO, Bruch's membrane opening; pCh, peripapillary choroid.

Investigative Ophthalmology & Visual Science

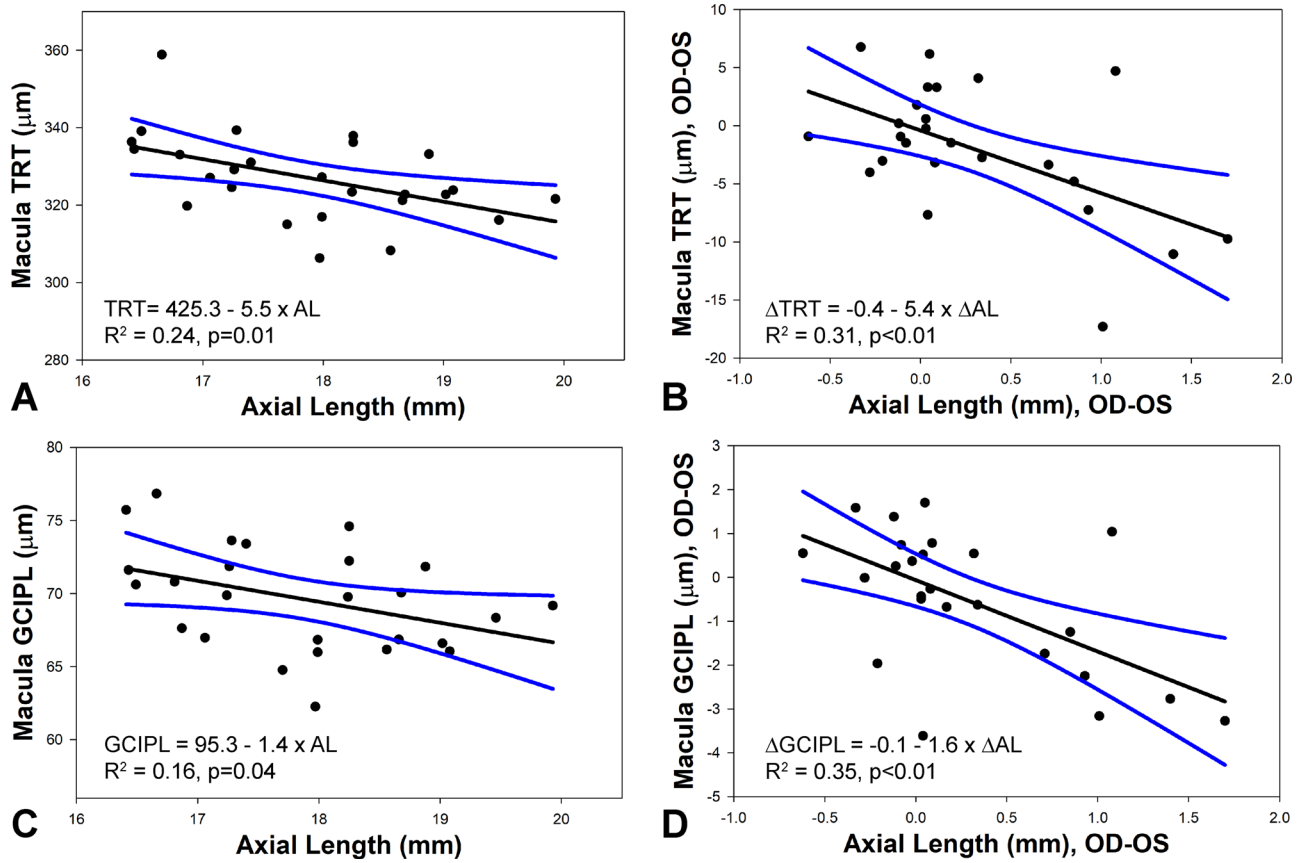

Figure 4. Right eye and inter-eye difference correlations with axial length and mTRT (**A, B**), and GCIPL thickness (**C, D**). *Blue lines* illustrate the 95% confidence interval for the slope of the function. GCIPL, ganglion cell inner plexiform layer; mTRT, macula total retinal thickness.

study suggest that stretching of axons from mild to moderate axial elongation alone has minimal effect on retinal ganglion cell content.

The relationship between choroid thickness and axial length/refractive error has been extensively studied, showing that longer or more myopic eyes have a thinner choroid.[73–76] In these previous studies, choroid thickness is most commonly measured in the macula region, where the changes are influenced by axial length and other factors, including, but not limited to defocus, age, medication use, and time of day.[77–83] The relationship between axial length and choroid thickness has also been reported for the peripapillary region,[84] and, as with previous studies, the current work suggests that longer eyes have a thinner peripapillary choroid, although this relationship was not appreciated when interocular comparisons were made (see Figs. 3G, 3F). The latter likely reflects the larger variability of this measure in comparison to the effect size for rhesus monkeys and our relatively small sample size, as the relationship between axial length and choroid thickness was also significant when only left eye data were analyzed ($R^2 = 0.50$, $P < 0.01$, plot not shown, see Supplementary Data File). Although several studies show that choroid thickness is not decreased in patients with open-angle glaucoma,[84–86] it is thinner in patients with peripapillary atrophy,[87] and could be associated with vascular compromise to the ONH.

In addition to the ONH and peripapillary region, OCT assessment of the macula region, including the inner retinal thickness, provides valuable information on retinal ganglion cell content in healthy and diseased eyes.[88,89] Although the association has a lot of variability, with more significant axial elongation, human studies suggest greater thinning of the total retinal thickness in the periphery.[3,90,91] For the macula region, whereas some studies show no relationship with axial length, others suggest a negative correlation with the nuclear layers, including the GCIPL, inner nuclear layer, and outer nuclear layer.[3–8,92–94] In the present study, both total retinal and GCIPL thickness were negatively correlated with axial length. The slope of the function was steeper for total retinal thickness than GCIPL thickness, suggesting greater outer than inner retinal thinning with axial elongation. Together with the ONH data, these findings suggest that although axial elongation does not result in retinal ganglion cell loss, the cell density is reduced in the macula region.

The study has several additional limitations to those already mentioned. The current data are cross-sectional in nature, and longitudinal changes, as demonstrated in other species, cannot be ascertained.[95] Whereas both the ONH and macula regions were imaged, widefield imaging could provide added information on the extent of retinal thinning with eccentricity with axial elongation. Due to the limited number of subjects, sector-based analysis was not performed for statistical reasons. Our laboratory has reported on the repeatability of most OCT metrics used for this study. However, in this cross-sectional study, we could not assess repeatability of new metrics, including the crescent area. Although assumptions can be made on cellular

Investigative Ophthalmology & Visual Science

content, the study did not quantify retrobulbar axon counts or retinal nuclear layer cell density. In addition, the study did not induce a pathological state to determine if morphological differences in longer versus shorter eyes place them at higher risk of disease. To address these limitations, our future studies will include longitudinal data collection, with glaucoma risk assessment when animals reach sexual maturity.

Conclusions

In young rhesus monkeys, longer axial lengths were associated with a series of ocular morphological changes, including larger BMO areas with a more anterior position of the lamina. Whereas circumpapillary RNFL thickness and ONH MRW were not related to axial length, the macula total retinal and GCIPL thicknesses were thinner in longer eyes. The associations were seen in right-eye only analyses, as well as in interocular comparisons, and collectively they support that axial elongation in developing eyes alters the posterior eye morphology. Whether or not these changes contribute to the onset and development of glaucoma remains to be studied.

Acknowledgments

Supported by NIH grants R01 EY029229, R01 EY003611, and P30 EY007551.

Disclosure: **Z. She**, None; **K.M. Beach**, None; **L.-F. Hung**, None; **L.A. Ostrin**, Zeiss Vision Care (C), Vyluma (C), Meta LLC (F); **E.L. Smith III**, patents on optical and pharmaceutical treatment strategies for myopia (P), SightGlass Vision (C), Treehouse Eyes (C); **N.B. Patel**, Heidelberg Engineering (S), Earl Smith - Vision CRC (F)

References

1. Holden BA, Fricke TR, Wilson DA, et al. Global prevalence of myopia and high myopia and temporal trends from 2000 through 2050. *Ophthalmology*. 2016;123:1036–1042.
2. Bullimore MA, Brennan NA. The underestimated role of myopia in uncorrectable visual impairment in the United States. *Sci Rep*. 2023;13:15283.
3. Chung YW, Choi MY, Kim JS, Kwon JW. The association between macular thickness and axial length in myopic eyes. *Biomed Res Int*. 2019;2019:8913582.
4. Read SA, Alonso-Caneiro D, Vincent SJ. Longitudinal changes in macular retinal layer thickness in pediatric populations: myopic vs non-myopic eyes. *PLoS One*. 2017;12:e0180462.
5. Jiang Z, Shen M, Xie R, Qu J, Xue A, Lu F. Interocular evaluation of axial length and retinal thickness in people with myopic anisometropia. *Eye Contact Lens*. 2013;39:277–282.
6. Lam DS, Leung KS, Mohamed S, et al. Regional variations in the relationship between macular thickness measurements and myopia. *Invest Ophthalmol Vis Sci*. 2007;48:376–382.
7. Hwang YH, Kim YY. Macular thickness and volume of myopic eyes measured using spectral-domain optical coherence tomography. *Clin Exp Optom*. 2012;95:492–498.
8. Luo HD, Gazzard G, Fong A, et al. Myopia, axial length, and OCT characteristics of the macula in Singaporean children. *Invest Ophthalmol Vis Sci*. 2006;47:2773–2781.
9. Read SA, Collins MJ, Vincent SJ, Alonso-Caneiro D. Choroidal thickness in myopic and nonmyopic children assessed with enhanced depth imaging optical coherence tomography. *Invest Ophthalmol Vis Sci*. 2013;54:7578–7586.
10. Nishida Y, Fujiwara T, Imamura Y, Lima LH, Kurosaka D, Spaide RF. Choroidal thickness and visual acuity in highly myopic eyes. *Retina*. 2012;32:1229–1236.
11. Harb E, Hyman L, Gwiazda J, et al. Choroidal thickness profiles in myopic eyes of young adults in the correction of Myopia Evaluation Trial Cohort. *Am J Ophthalmol*. 2015;160:62–71.e62.
12. Xiong S, He X, Deng J, et al. Choroidal thickness in 3001 Chinese children aged 6 to 19 years using swept-source OCT. *Sci Rep*. 2017;7:45059.
13. Małyszczak A, Żyto M, Przeździecka-Dołyk J, Misiuk-Hojło M. Macular vascularity and ganglion cell complex parameters in the young adults with myopia and progressive myopia. *Clin Ophthalmol*. 2023;17:561–570.
14. Shuaib A, Salem SA, Elnahry AG, Ghalwash DA, Mohalhal AA. Correlation of the macular microvasculature to the axial length in pediatric patients with high axial refractive errors. *Eye (Lond)*. 2024;38:507–513.
15. Jonas JB. Optic disk size correlated with refractive error. *Am J Ophthalmol*. 2005;139:346–348.
16. Oliveira C, Harizman N, Girkin CA, et al. Axial length and optic disc size in normal eyes. *Br J Ophthalmol*. 2007;91:37–39.
17. Chan PP, Zhang Y, Pang CP. Myopic tilted disc: mechanism, clinical significance, and public health implication. *Front Med (Lausanne)*. 2023;10:1094937.
18. Seo JH, Kim TW, Weinreb RN. Lamina cribrosa depth in healthy eyes. *Invest Ophthalmol Vis Sci*. 2014;55:1241–1251.
19. Chui TY, Zhong Z, Burns SA. The relationship between peripapillary crescent and axial length: implications for differential eye growth. *Vision Res*. 2011;51:2132–2138.
20. Mitchell P, Hourihan F, Sandbach J, Wang JJ. The relationship between glaucoma and myopia: the Blue Mountains Eye Study. *Ophthalmology*. 1999;106:2010–2015.
21. Perera SA, Wong TY, Tay W-T, Foster PJ, Saw S-M, Aung T. Refractive error, axial dimensions, and primary open-angle glaucoma: the Singapore Malay Eye Study. *Arch Ophthalmol*. 2010;128:900–905.
22. Perkins ES, Phelps CD. Open angle glaucoma, ocular hypertension, low-tension glaucoma, and refraction. *Arch Ophthalmol*. 1982;100:1464–1467.
23. Vijaya L, Rashima A, Panday M, et al. Predictors for incidence of primary open-angle glaucoma in a South Indian population: the Chennai Eye Disease Incidence Study. *Ophthalmology*. 2014;121:1370–1376.
24. Wong TY, Klein BE, Klein R, Knudtson M, Lee KE. Refractive errors, intraocular pressure, and glaucoma in a white population. *Ophthalmology*. 2003;110:211–217.
25. Xu L, Wang Y, Wang S, Wang Y, Jonas JB. High myopia and glaucoma susceptibility the Beijing Eye Study. *Ophthalmology*. 2007;114:216–220.
26. Casson RJ, Gupta A, Newland HS, et al. Risk factors for primary open-angle glaucoma in a Burmese population: the Meiktila Eye Study. *Clin Exp Ophthalmol*. 2007;35:739–744.
27. Ha A, Kim CY, Shim SR, Chang IB, Kim YK. Degree of myopia and glaucoma risk: a dose-response meta-analysis. *Am J Ophthalmol*. 2022;236:107–119.
28. Boote C, Sigal IA, Grytz R, Hua Y, Nguyen TD, Girard MJA. Scleral structure and biomechanics. *Prog Retin Eye Res*. 2020;74:100773.
29. Downs JC. Optic nerve head biomechanics in aging and disease. *Exp Eye Res*. 2015;133:19–29.
30. Raviola E, Wiesel TN. An animal model of myopia. *N Engl J Med*. 1985;312:1609–1615.
31. Troilo D, Smith EL, III, Nickla DL, et al. IMI – Report on experimental models of emmetropization and myopia. *Invest Ophthalmol Vis Sci*. 2019;60:M31–M88.

Investigative Ophthalmology & Visual Science

32. She Z, Hung LF, Arumugam B, Beach KM, Smith EL, 3rd. The development of and recovery from form-deprivation myopia in infant rhesus monkeys reared under reduced ambient lighting. *Vision Res*. 2021;183:106–117.
33. She Z, Hung LF, Arumugam B, Beach KM, Smith EL. Effects of low intensity ambient lighting on refractive development in infant rhesus monkeys (Macaca mulatta). *Vision Res*. 2020;176:48–59.
34. She Z, Hung LF, Arumugam B, Beach KM, Smith Iii EL. The effects of reduced ambient lighting on lens compensation in infant rhesus monkeys. *Vision Res*. 2021;187:14–26.
35. Smith EL, 3rd, Hung LF. The role of optical defocus in regulating refractive development in infant monkeys. *Vision Res*. 1999;39:1415–1435.
36. Qiao-Grider Y, Hung L-F, C-S Kee, Ramamirtham R, Smith EL, III. Recovery from form-deprivation myopia in rhesus monkeys. *Invest Ophthalmol Vis Sci*. 2004;45:3361–3372.
37. Patel NB, Hung LF, Harwerth RS. Postnatal maturation of the fovea in Macaca mulatta using optical coherence tomography. *Exp Eye Res*. 2017;164:8–21.
38. Patel NB, Carter-Dawson L, Frishman LJ. Neuroretinal rim response to transient intraocular pressure challenge predicts the extent of retinal ganglion cell loss in experimental glaucoma. *Invest Ophthalmol Vis Sci*. 2023;64:30.
39. Srinivasan VV, Das S, Patel N. Widefield OCT imaging for quantifying inner retinal thickness in the nonhuman primate. *Transl Vis Sci Technol*. 2022;11:12.
40. Chen L-C, Papandreou G, Schroff F, Adam H. Rethinking atrous convolution for semantic image segmentation. *arXiv preprint arXiv:170605587* 2017.
41. He K, Zhang X, Ren S, Sun J. Deep residual learning for image recognition. *2016 IEEE Conference on Computer Vision and Pattern Recognition (CVPR)*; 2016:770–778.
42. Girard MJ, Strouthidis NG, Ethier CR, Mari JM. Shadow removal and contrast enhancement in optical coherence tomography images of the human optic nerve head. *Invest Ophthalmol Vis Sci*. 2011;52:7738–7748.
43. Patel NB, Luo X, Wheat JL, Harwerth RS. Retinal nerve fiber layer assessment: area versus thickness measurements from elliptical scans centered on the optic nerve. *Invest Ophthalmol Vis Sci*. 2011;52:2477–2489.
44. Mwanza J-C, Durbin MK, Budenz DL, et al. Profile and predictors of normal ganglion cell–inner plexiform layer thickness measured with frequency-domain optical coherence tomography. *Invest Ophthalmol Vis Sci*. 2011;52:7872–7879.
45. Hendrickson A, Kupfer C. The histogenesis of the fovea in the macaque monkey. *Invest Ophthalmol Vis Sci*. 1976;15:746–756.
46. Kirby MA, Steineke TC. Morphogenesis of retinal ganglion cells: a model of dendritic, mosaic, and foveal development. *Perspect Dev Neurobiol*. 1996;3:177–194.
47. La Vail MM, Rapaport DH, Rakic P. Cytogenesis in the monkey retina. *J Comp Neurol*. 1991;309:86–114.
48. Rapaport DH, Rakic P, LaVail MM. Spatiotemporal gradients of cell genesis in the primate retina. *Perspect Dev Neurobiol*. 1996;3:147–159.
49. Packer O, Hendrickson AE, Curcio CA. Development redistribution of photoreceptors across the Macaca nemestrina (pigtail macaque) retina. *J Comp Neurol*. 1990;298:472–493.
50. Rimmer S, Keating C, Chou T, et al. Growth of the human optic disk and nerve during gestation, childhood, and early adulthood. *Am J Ophthalmol*. 1993;116:748–753.
51. Patel A, Purohit R, Lee H, et al. Optic nerve head development in healthy infants and children using handheld spectral-domain optical coherence tomography. *Ophthalmology*. 2016;123:2147–2157.
52. Budenz DL. Symmetry between the right and left eyes of the normal retinal nerve fiber layer measured with optical coherence tomography (an AOS thesis). *Trans Am Ophthalmol Soc*. 2008;106:252–275.
53. Zhang XJ, Wang YM, Jue Z, et al. Interocular symmetry in retinal nerve fiber layer thickness in children: the Hong Kong Children Eye Study. *Ophthalmol Ther*. 2023;12:3373–3382.
54. Song MY, Hwang YH. Interocular symmetry of optical coherence tomography parameters in healthy children and adolescents. *Sci Rep*. 2022;12:653.
55. Rimmer S, Keating C, Chou T, et al. Growth of the human optic disk and nerve during gestation, childhood, and early adulthood. *Am Journal of Ophthalmol*. 1993;116:748–753.
56. Zhang Q, Xu L, Wei WB, Wang YX, Jonas JB. Size and shape of Bruch's membrane opening in relationship to axial length, gamma zone, and macular Bruch's membrane defects. *Invest Ophthalmol Vis Sci*. 2019;60:2591–2598.
57. KhalafAllah MT, Fuchs PA, Nugen F, et al. Longitudinal changes of Bruch's membrane opening, anterior scleral canal opening, and border tissue in experimental juvenile high myopia. *Invest Ophthalmol Vis Sci*. 2023;64:2.
58. Jeoung JW, Yang H, Gardiner S, et al. Optical coherence tomography optic nerve head morphology in myopia I: implications of anterior scleral canal opening versus Bruch membrane opening offset. *Am J Ophthalmol*. 2020;218:105–119.
59. Jeoung JW, Yang H, Gardiner S, et al. Optical coherence tomography optic nerve head morphology in myopia i: implications of anterior scleral canal opening versus Bruch membrane opening offset. *Am J Ophthalmol*. 2020;218:105–119.
60. Wang YX, Panda-Jonas S, Jonas JB. Optic nerve head anatomy in myopia and glaucoma, including parapapillary zones alpha, beta, gamma and delta: histology and clinical features. *Prog Retin Eye Res*. 2021;83:100933.
61. Hill D, Heitmar R, Logan NS. Size and position of the optic disc crescent in a white European population with myopia. *Ophthalmic Physiol Opt*. 2022;42:1115–1123.
62. Jonas JB, Fernández MC, Naumann GO. Correlation of the optic disc size to glaucoma susceptibility. *Ophthalmology*. 1991;98:675–680.
63. Jonas JB, Martus P, Budde WM. Anisometropia and degree of optic nerve damage in chronic open-angle glaucoma. *Am J Ophthalmol*. 2002;134:547–551.
64. Zangwill LM, Weinreb RN, Beiser JA, et al. Baseline topographic optic disc measurements are associated with the development of primary open-angle glaucoma: the Confocal Scanning Laser Ophthalmoscopy Ancillary Study to the Ocular Hypertension Treatment Study. *Arch Ophthalmol*. 2005;123:1188–1197.
65. Burk RO, Rohrschneider K, Noack H, Völcker HE. Are large optic nerve heads susceptible to glaucomatous damage at normal intraocular pressure? A three-dimensional study by laser scanning tomography. *Graefes Arch Clin Exp Ophthalmol*. 1992;230:552–560.
66. Vurgese S, Panda-Jonas S, Jonas JB. Scleral thickness in human eyes. *PLoS One*. 2012;7:e29692.
67. Ren R, Wang N, Li B, et al. Lamina cribrosa and peripapillary sclera histomorphometry in normal and advanced glaucomatous Chinese eyes with various axial length. *Invest Ophthalmol Vis Sci*. 2009;50:2175–2184.
68. Jonas JB, Berenshtein E, Holbach L. Lamina cribrosa thickness and spatial relationships between intraocular space and cerebrospinal fluid space in highly myopic eyes. *Invest Ophthalmol Vis Sci*. 2004;45:2660–2665.
69. Kang SH, Hong SW, Im S, Lee S, Ahn MD. Effect of myopia on the thickness of the retinal nerve fiber layer measured by

Investigative Ophthalmology & Visual Science

Cirrus HD optical coherence tomography. *Invest Ophthalmol Vis Sci*. 2010;51:4075–4083.
70. Bayraktar S, Bayraktar Z, Yilmaz OF. Influence of scan radius correction for ocular magnification and relationship between scan radius with retinal nerve fiber layer thickness measured by optical coherence tomography. *J Glaucoma*. 2001;10:163–169.
71. Huang D, Chopra V, Lu AT-H, et al. Does optic nerve head size variation affect circumpapillary retinal nerve fiber layer thickness measurement by optical coherence tomography? *Invest Ophthalmol Vis Sci*. 2012;53:4990–4997.
72. Fortune B, Hardin C, Reynaud J, et al. Comparing optic nerve head rim width, rim area, and peripapillary retinal nerve fiber layer thickness to axon count in experimental glaucoma. *Invest Ophthalmol Vis Sci*. 2016;57:Oct404–Oct412.
73. Ho M, Liu DT, Chan VC, Lam DS. Choroidal thickness measurement in myopic eyes by enhanced depth optical coherence tomography. *Ophthalmology*. 2013;120:1909–1914.
74. Flores-Moreno I, Lugo F, Duker JS, Ruiz-Moreno JM. The relationship between axial length and choroidal thickness in eyes with high myopia. *Am J Ophthalmol*. 2013;155:314–319.e311.
75. Read SA, Collins MJ, Vincent SJ, Alonso-Caneiro D. Choroidal thickness in myopic and nonmyopic children assessed with enhanced depth imaging optical coherence tomography. *Invest Ophthalmol Vis Sci*. 2013;54:7578–7586.
76. Gupta P, Saw S-M, Cheung CY, et al. Choroidal thickness and high myopia: a case–control study of young Chinese men in Singapore. *Acta Ophthalmologica*. 2015;93:e585–e592.
77. Wallman J, Wildsoet C, Xu A, et al. Moving the retina: choroidal modulation of refractive state. *Vision Res*. 1995;35:37–50.
78. Wildsoet C, Wallman J. Choroidal and scleral mechanisms of compensation for spectacle lenses in chicks. *Vision Res*. 1995;35:1175–1194.
79. Wang D, Chun RK, Liu M, et al. Optical defocus rapidly changes choroidal thickness in schoolchildren. *PLoS One*. 2016;11:e0161535.
80. Shao L, Xu L, Wei WB, et al. Visual acuity and subfoveal choroidal thickness: the Beijing Eye Study. *Am J Ophthalmol*. 2014;158:702–709.e701.
81. Yeung SC, Park JY, Park D, You Y, Yan P. The effect of systemic and topical ophthalmic medications on choroidal thickness: a review. *Br J Clin Pharmacol*. 2022;88:2673–2685.
82. Delshad S, Collins MJ, Read SA, Vincent SJ. The human axial length and choroidal thickness responses to continuous and alternating episodes of myopic and hyperopic blur. *PLoS One*. 2020;15:e0243076.
83. Burfield HJ, Patel NB, Ostrin LA. Ocular biometric diurnal rhythms in emmetropic and myopic adults. *Invest Ophthalmol Vis Sci*. 2018;59:5176–5187.
84. Read SA, Alonso-Caneiro D, Vincent SJ, Collins MJ. Peripapillary choroidal thickness in childhood. *Exp Eye Res*. 2015;135:164–173.
85. Wang W, Zhang X. Choroidal thickness and primary open-angle glaucoma: a cross-sectional study and meta-analysis. *Invest Ophthalmol Vis Sci*. 2014;55:6007–6014.
86. Zhang C, Tatham AJ, Medeiros FA, Zangwill LM, Yang Z, Weinreb RN. Assessment of choroidal thickness in healthy and glaucomatous eyes using swept source optical coherence tomography. *PLoS One*. 2014;9:e109683.
87. Sullivan-Mee M, Patel NB, Pensyl D, Qualls C. Relationship between juxtapapillary choroidal volume and beta-zone parapapillary atrophy in eyes with and without primary open-angle glaucoma. *Am J Ophthalmol*. 2015;160:637–647.e631.
88. Mwanza JC, Oakley JD, Budenz DL, Anderson DR, Cirrus Optical Coherence Tomography Normative Database Study Group. Ability of cirrus HD-OCT optic nerve head parameters to discriminate normal from glaucomatous eyes. *Ophthalmology*. 2011;118:241–248.e241.
89. Antwi-Boasiako K, Carter-Dawson L, Harwerth R, Gondo M, Patel N. The relationship between macula retinal ganglion cell density and visual function in the nonhuman primate. *Invest Ophthalmol Vis Sci*. 2021;62:5.
90. Jonas JB, Xu L, Wei WB, et al. Retinal thickness and axial length. *Invest Ophthalmol Vis Sci*. 2016;57:1791–1797.
91. Panda-Jonas S, Jonas JB, Jonas RA. Photoreceptor density in relation to axial length and retinal location in human eyes. *Sci Rep*. 2022;12:21371.
92. Szigeti A, Tátrai E, Varga BE, et al. The effect of axial length on the thickness of intraretinal layers of the macula. *PLoS One*. 2015;10:e0142383.
93. Palazon-Cabanes A, Palazon-Cabanes B, Rubio-Velazquez E, Lopez-Bernal MD, Garcia-Medina JJ, Villegas-Perez MP. Normative database for all retinal layer thicknesses using SD-OCT posterior pole algorithm and the effects of age, gender and axial lenght. *J Clin Med*. 2020;9:3317.
94. Ooto S, Hangai M, Tomidokoro A, et al. Effects of age, sex, and axial length on the three-dimensional profile of normal macular layer structures. *Invest Ophthalmol Vis Sci*. 2011;52:8769–8779.
95. KhalafAllah MT, Fuchs PA, Nugen F, et al. Heterogenous thinning of peripapillary tissues occurs early during high myopia development in juvenile tree shrews. *Exp Eye Res*. 2024;240:109824.

Investigative Ophthalmology & Visual Science